A sensor network for integrated Space Traffic Management for Australia

Edwin G. W. Peters [1]
[1]UNSW Canberra Space, Canberra, Australia
Melrose Brown [1], Andrew Lambert [1], Lauren Glina [1], Timothy Bateman [1], Ed Kruzins [1], Rabbia Saleem [1], Travis Bessell [2], Tim Spitzer [2], Tom Wang [2], Kriti Tripathi [2], Damian Huxtable [2], Michael Soire [2], Simon Zinsli [2], Thomas Powles [2], Isabella Federle [2], Mark Aragon [3], Adam Haskard [3], Mark Thompson [4], Warren Nielsen [4], Russell Boyce [1]
[1]UNSW Canberra Space, [2]Clearbox Systems, [3]Bluerydge, [4] Capricorn Space

ABSTRACT

The number of near-Earth resident space objects is set to grow by an order of magnitude by the end of the decade. Developing new space traffic management (STM) systems is critical to mitigate the risk of on-orbit collisions from the rapidly growing population of spacecraft. We present an early version of our proposed architecture for an STM system that combines the use of passive radio frequency (RF) and optical sensors that, combined with dynamic tasking procedures, lays the foundation for next generation STM networks. Optical and passive RF data will be fused for orbit determination (OD), resident space object (RSO) characterisation, and initial orbit determination (IOD).

This paper presents some of the progress as part of the Australian Government funded cooperative research centre project (CRC-P) project titled "A sensor network for integrated space traffic management for Australia" with some early results as well as a case study of manoeuvre tracking of the UNSW Canberra Space built and operated M2-A and M2-B spacecraft.

1. INTRODUCTION

The number of near-Earth resident space objects is set to grow by an order of magnitude by the end of the decade [4, 7, 8]. Developing new STM systems is critical to mitigate the risk of on-orbit collisions from the rapidly growing population of spacecraft. Future STM systems must contend with not only an increase in the number of objects in orbit but an increasingly dynamic space environment, where low-thrust electric propulsion systems combined with artificial intelligence-based spacecraft navigation systems result in levels of manoeuvrability that were not envisioned during the design of existing STM systems. The emergence of commercial space actors as the primary owner/operators of future satellite technology has driven the transition of STM from a military responsibility to the civilian realm. It is therefore critical that new space domain awareness (SDA) sensors and mission systems are developed from the civilian and commercial sector to meet both the technical and business/use case challenges that the changing utilisation of the space domain requires.

Australia has embarked on a dedicated effort in recent years to rise to the global SDA challenge, seeking to exploit our advantages in geography and dark/RF quiet skies through several government initiatives. The work presented here shall outline and update progress on the research and development of a new integrated passive RF and optical SDA sensor network solution under the Australian Government's round 9 cooperative research centre project (CRC-P) "A sensor network for integrated space traffic management for Australia". The program represents a tight collaboration between industry and academic partners to stimulate improved levels of translation from academic research into the commercial sector.

The CRC-P is a collaboration between UNSW Canberra Space, Clearbox Systems, Capricorn Space and Bluerydge. Clearbox Systems is building and deploying the SpaceAware passive RF network comprising of sensor sites located in the Australian Capital Territory (ACT), New South Wales, South Australia and Western Australia. The system will seek to detect actively transmitting satellites in the very-high frequency (VHF), ultra-high frequency (UHF), S, X and Ku bands, using a combination of omnidirectional and directional antennas. While the frequency offset

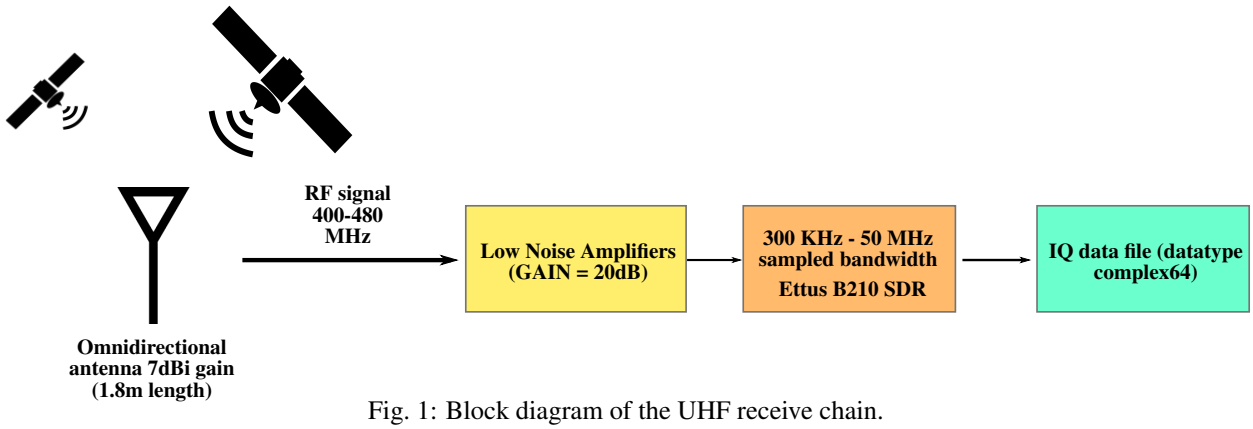

Fig. 1: Block diagram of the UHF receive chain.

due to Doppler for a satellite can be measured using a single receiving antenna, multiple receivers that are either co-located or geographically dispersed, can estimate the angle of arrival and range using array processing as well as time and frequency difference of arrival methods. The combination of omnidirectional and directional antennas allows for simultaneous monitoring of the entire horizon, while allowing tracking of specific objects for more accurate measurements. The cost and power requirements are significantly reduced compared to active RF systems, allowing a cost-effective geographically dispersed roll-out. The passive RF systems rely on the objects of interest actively transmitting and their beam width within the field of view of the sensor network. Coupling the system with optical telescopes provides the opportunity to enhance the SDA information available for any given object. The research conducted during the CRC-P program will exploit UNSW Canberra's 36 cm, 2° field of view 'VIPER' telescope to provide tracking and characterization data to complement the passive RF sensor network. Capricorn Space operates a ground station as a service capability with a sensor site located in Mingenew, WA. Part of the CRC-P will demonstrate how existing satellite communication hardware can be repurposed into SDA sensors. Bluerydge is ensuring that the design and deployment of the sensor network and data generated from it is secure by applying their extensive cyber security knowledge. Following development and commissioning of the respective RF and optical systems, work shall commence on research to explore how metric and characterisation data can be exchanged between the optical and RF systems to extend the knowledge of space objects beyond what either system could independently yield.

This paper presents details of the program's current development, sensor network architecture and preliminary results for select satellites. Preliminary results from example observations performed during the sprint advanced concept training (SACT) event [5] of the UNSW Canberra Space built and operated "M2" formation flying CubeSat mission in the optical and RF spectrum are compared to two line element (TLE) information during crossover and close-proximity manoeuvring executed through a sequence of differential aerodynamic drag manoeuvres. The methods used and algorithms implemented for extracting range-rate data from the passive RF signals and the approaches applied to those data for OD are demonstrated. The preliminary results presented in this paper highlight opportunities for characterisation data to detect changes in spacecraft state that in future work can be exploited to improve OD and manoeuvre detection algorithms.

This paper is organised as follows: Section 2 presents an overview of the passive RF sensor sites followed by an overview of the optical sensors in Section 3. Next, the RF signalling processing algorithm is presented and demonstrated in Section 4. Section 5 demonstrates data aggregation and OD methods used, and to be used in the project. The case-study of the SACT event where both optical and passive RF sensors were used is demonstrated in Section 6 before summarising in Sections 7 and 8.

2. PASSIVE RF SENSOR NETWORK

UNSW Canberra operates three sensor sites, where one is located on-campus, one 80 km North-West in Yass, and a test site at Captains Flat 25 km East with Clearbox Systems operating another two sensor sites in Adelaide and Mingenew. The sensor sites have a variety of antennas, both directional and omni-directional, capable of receiving numerous frequency bands, including:

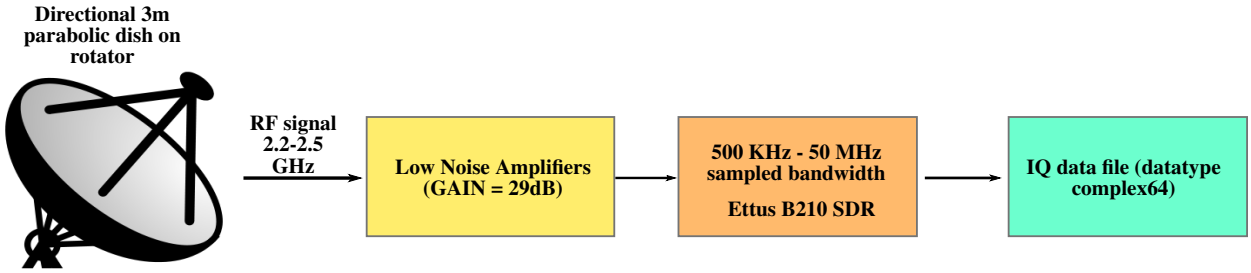

Fig. 2: Block diagram of the S band receive chain.

Fig. 3: The UNSW Falcon telescope (part of the USAFA-led Falcon Telescope Network).

Fig. 4: The remotely operated, self-contained UNSW VIPER telescope.

- Ku band (10.7-12.75 GHz)
- S band (2.3-2.7 GHz)
- X band (8.0-8.4 GHz)
- UHF (400-470 MHz)
- VHF (130-150 MHz).

The RF signals are downconverted, digitised and captured using software defined radio (SDR) units. These SDRs feature up to four simultaneous RF inputs which are selectable via software control. A GPS disciplined oscillator is utilised to ensure accurate time tagging of data. The Ku band RF signal is downconverted using a low-noise block converter (LNB) to convert the RF to an intermediate frequency (IF) compatible with the Ettus B210 SDR. The Ku band and S band systems utilise SPID antenna rotators to track signals from GEO and LEO satellites. The omni-directional nature of the UHF antenna allows low earth orbit (LEO) satellites transmitting in the UHF band to be received without needing a rotator.

A block diagram of the UHF receive chain present at the UNSW Canberra campus and Captains Flat sites is depicted in Fig. 1. The low-noise amplifiers (LNAs) used are co-located with the antenna. While the S band capabilities at the UNSW Canberra campus site are limited due to the small size of the aperture, the satellite communication site at Yass features a 3 m parabolic aperture, with the block diagram depicted in Fig. 2.

3. WIDEFIELD AND NARROWFIELD OPTICAL TELESCOPES

UNSW Canberra Space operates a number of telescopes for SDA, and collaborates with partners in Western Australia and New Zealand as well as those involved with the Falcon Telescope Network [2]. Figure 3 depicts the Falcon telescope that is part of the global Falcon Telescope Network [2]. The wide field-of-view VIPER telescope is depicted in Fig. 4.

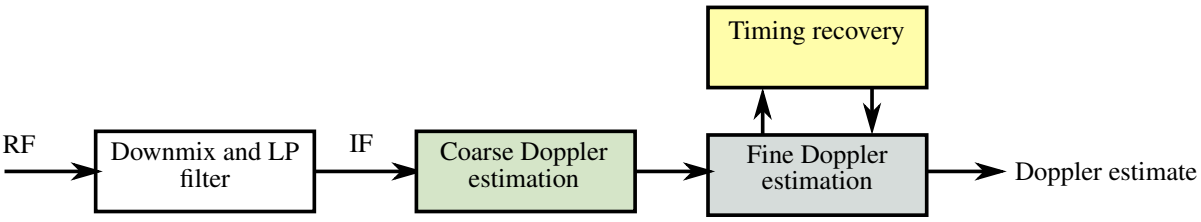

Fig. 5: Simplified flow chart of the proposed passive RF Doppler estimation SDR algorithm.

All telescopes are capable of staring, sidereal, and rate-tracking mode of detection, however the wider field of view of the VIPER telescope lends itself to survey operation, and the Falcon to rate-tracking. The automation of these is developed by USAFA CSOC for the Falcon, and by ourselves for VIPER and its use with passive RF scheduled observations. Where possible commercial off the shelf (COTS) equipment and software are exploited to facilitate this.

3.1 Falcon

The UNSW Canberra Falcon telescope is a 0.5 m f8.1 main telescope with a 4m focal length. This is accompanied by an Astrotech AT106 0.1m f6.5 refractive viewfinder telescope with focal length 690 mm. The main telescope is equipped with a standard filter wheel with common spectral filters and a 100 lp/mm diffraction grating for slit-less spectroscopy.commercial

Both of the currently installed cameras on the UNSW Falcon telescope are cooled: Atik 414ex (SONY ICX825 sensor with 1380x1040 6.46 µm square pixels) with an option to swap in a CeleX5 Event Based Image Sensor for high temporal rate observations. The pixel field of view from the main telescope is 1.6 µrad, and 6.5 µrad in the viewfinder. Observations can be automatically or manually operated.

3.2 VIPER

The VIPER telescope facility incorporates a cooled Celestron 36 cm Rowe-Ackermann Schmidt Astrograph (f/2.2) on a Software Bisque "Paramount MX+" GEM robotic telescope mount. The detector is a Ximea CB120MG-CM-X8G3 monochrome CMOS camera, (CMOSIS CMV12000 sensor with a resolution of 4096x3072 pixels) with a pixel scale of 1.44 arcsec/pixel, providing a wide field capture of around 2° across the frame diagonal. The camera is directly connected, via a high-speed PCIe bus, to an NVIDIA Jetson TX2 system on a chip (SOC) (mounted atop the optical telescope assembly), enabling the use of innovative AI-at-the-edge and real-time GPU image processing algorithms.

The installation is intended to be self-contained and remotely operated via VPN internet connection. It is powered by solar panels with battery storage.

4. RF SIGNAL PROCESSING - DOPPLER ANALYSIS

Passive RF observations rely on capturing of signals emitted or reflected by objects in space, and extract positional and identification data from these. In the current stage of this project, the focus is on the capture and processing of signals emitted directly by orbiting spacecraft, such as their communication signals and/or periodic beaconing signals.

Passive RF tracking can be done using a single station with one or multiple antennas or multiple geographically dispersed stations with one or multiple antennas at each station. When only a single aperture is used for receiving RF signals at a single station, the only direct information that can be extracted from the received RF signal is the frequency offset caused by the Doppler effect due to the relative velocity between the transmitter (satellite) and receiver (ground station) [1, 6]. The Doppler frequency can be estimated and the range rate computed from this can be used for OD using existing tools. Multiple co-located receivers at one receiver station can be used to determine the angle of arrival of a emitted signal. Passive multi-station methods utilise geographically dispersed receivers. With the appropriate synchronisation, the time and frequency of observations between stations will differ. The emitter's location can then be determined through the difference of the arrival frequencies and times as well as the geometry of the receivers. Typical methods within this category are time difference of arrival (TDoA) and frequency difference of arrival (FDoA) [3,6,9].

At the current stage of the project, we process data at individual stations using SDRs and estimate the Doppler frequency offset of the received signal using a variety of methods. The method most frequently used utilizes so-called

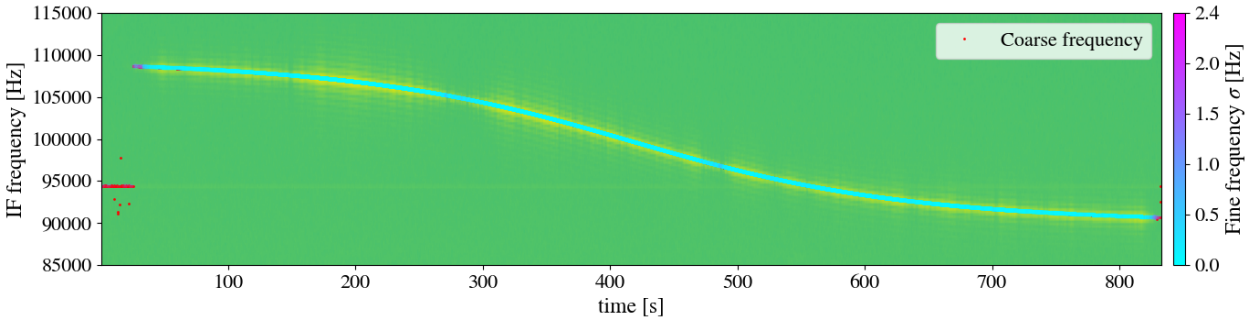

Fig. 6: Waterfall of Saral (NID 39086) with coarse and fine frequency estimation overlayed. The colour intensity of the fine estimate indicates the standard deviation.

matched filters, which are templates of the expected signal, to estimate the frequency offset of the received signal. A simplified flow diagram of the algorithm is depicted in Fig. 5. Further details on this algorithm are found in [10]. The output of the algorithm for a Saral pass are shown in Fig. 6. While the matched filter SDR Doppler estimation algorithm requires a-priori knowledge of the modulation scheme and data rate of the signal, the Doppler estimates feature a high time and frequency accuracy compared to the signal to noise ratio (SNR) of the received RF signal.

5. MISSION DATA AGGREGATION

Another critical part of the project includes data aggregation from optical and passive RF modules for a improved SDA of spacecraft. The combined data is expected to play an enhanced role in the investigation and monitoring of space mission activities such as OD. GPS, range rate, TDoA, FDoA as well as optical and RF based angle of arrival (AOA) are mainly the different data sets acquired as mentioned in Section 4. This project is aimed to adopt the following approaches on the datasets for space situational awareness:

5.1 Classical approaches for SDA

Firstly, the traditional estimation technique such as batch least squares is deployed on the range rate passive RF data for OD. Figure 7 plots the logarithmic range rate difference for the computed and observed values of the LEO spacecraft Saral (NID 39086) over two passes versus the time in UTC. These results were acquired for Saral passes on 2022-08-01 via UHF obtained at the Captains Flat test site in New South Wales. The computed range rate data is obtained from an orbit propagation using an TLE from 9th May 2022. As illustrated in Fig. 7, the difference is reducing for every iteration, reducing the mean absolute residual between the computed orbit and the measured data to 0.5 m/s. The batch least squares estimator solves for the spacecraft initial position, velocity, and drag coefficient. The state is propagated using an adaptive step, ninth order Runge-Kutta integrator with eighth order error control, using the EGM-96 gravity model set to 40th degree and order. Sun and Moon point masses and the MSIS-90 atmospheric model are employed. A regularly updated Center for Space Standards and Innovation space weather file is used as input to the MSIS-90 atmosphere model and a spherical drag model assumed. An orbit error covariance of 50 m and 50 m/s are applied to the initial orbit state.

5.2 Learning-based techniques for SDA

It is anticipated that with a growing population of spacecraft, the tracking, identification, and characterisation of these becomes increasingly difficult. Also, data aggregation itself is a high degree complex problem when dealing with the large number of entities. The computational complexity of traditional methods is too high to address this multi-dimensional, complex, and dynamic problem for the space network. Artificial intelligence and machine learning algorithms appeal as a suitable approach to address this problem. Moreover, learning-based algorithms can provide cost effective, less-computationally intensive and robust solutions for aggregating and analysing data for SDA.

6. SPRINT ADVANCED CONCEPT TRAINING

UNSW Canberra has been participating in SACT exercises. In 2019 a new international experimentation series called the ”Commercial Sprint Advanced Concept Training” evolved [5]. It serves as an ”innovation and collaboration test

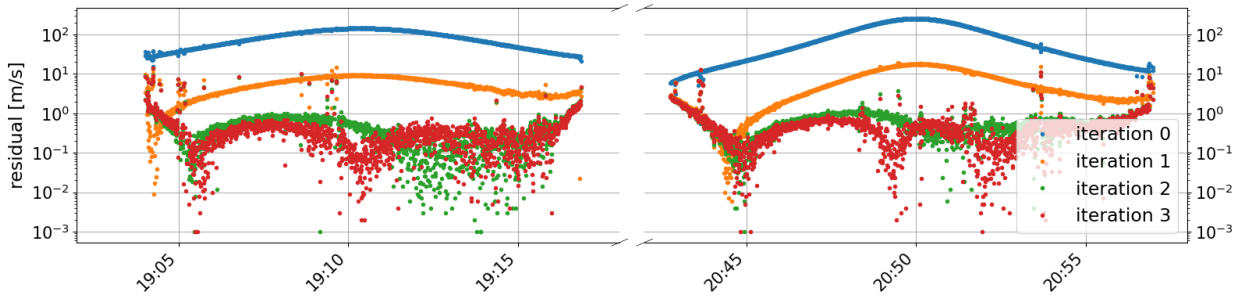

Fig. 7: The range rate residual of computed and observed range rate for Saral over two passes. The AOS was 2022-08-01. Note the logarithmic scaling on the vertical axis.

bed" for advancing all aspects of space operations.

6.1 UNSW Canberra M2 CubeSat Mission

The UNSW Canberra space built and operated M2 CubeSat mission consists of two 6U CubeSats launched conjointly as a single 12U CubeSat. In September last year, the conjoint M2 spacecraft separated into two 6U CubeSats M2-A and M2-B. These have been flying in formation since then. Due to the lack of propulsion on the M2 spacecraft, the formation is maintained and adjusted by applying high and low drag manoeuvres taking advantage of the thin particle density in the LEO environment.

During a SACT exercise in August 2022, UNSW Canberra commanded the M2-A and M2-B spacecraft to swap order in the formation. During this manoeuvre, the M2-A spacecraft that was trailing M2-B would fly in a low drag configuration while the leading spacecraft, M2-B, would fly in a high drag configuration. The spacecraft would pass each other with a relative distance in the range of 10s of meters. To the best of our knowledge, classical observation methods such as bi-static radar, are unable to accurately identify and track the spacecraft when in such close proximity to each other. While the speed of the manoeuvres was sufficiently small for up to date TLEs to remain usable, the accuracy of TLEs tend to be within kilometers, which is significantly larger than the distance between the spacecraft at their closest crossover distance.

We utilised passive RF and optical observations to identify and determine the position between the spacecraft. For the passive RF tracking, we instructed the spacecraft to emit continuous waves (carriers) on S band at a 200 kHz frequency offset to each other at certain communication passes. These RF signals were collected using our S band antenna at the Yass ground station.

The optical data was collected from the UNSW Canberra Falcon and VIPER telescopes. Both spacecraft were in view of the telescopes for a few days around the crossover.

Variations in the received signal strength, and thereby the SNR in both the optical and passive RF measurements indicate a stability assessment of the spacecraft.

6.2 Characterisation of M2 Formation Flying via passive RF S band observations

For the passive RF observations, the spacecraft were commanded to transmit a continuous wave on S band at a ±100 kHz offset from their centre frequency. These signals were recorded on the ground using a 3 m parabolic S band receiver, located at Yass. Figure 9 shows a spectrogram of a RF recording. The two horizontal lines with a sigmoid shape are the two tones emitted by the M2-A and M2-B spacecraft respectively. The horizontal lines are caused by local in-band interference.

The initial analysis estimates the distance between the spacecraft through the difference in the time of closest approach (TCA) of M2-A and M2-B. The TCA is measured using two methods as explained next.

6.2.1 Methodology

Figure 8 shows the processing flow of the distance estimation. It is worth noting that this is a crude analysis done in a limited time after the satellite passes. A more accurate detailed analysis is to be considered for future work. The *find*

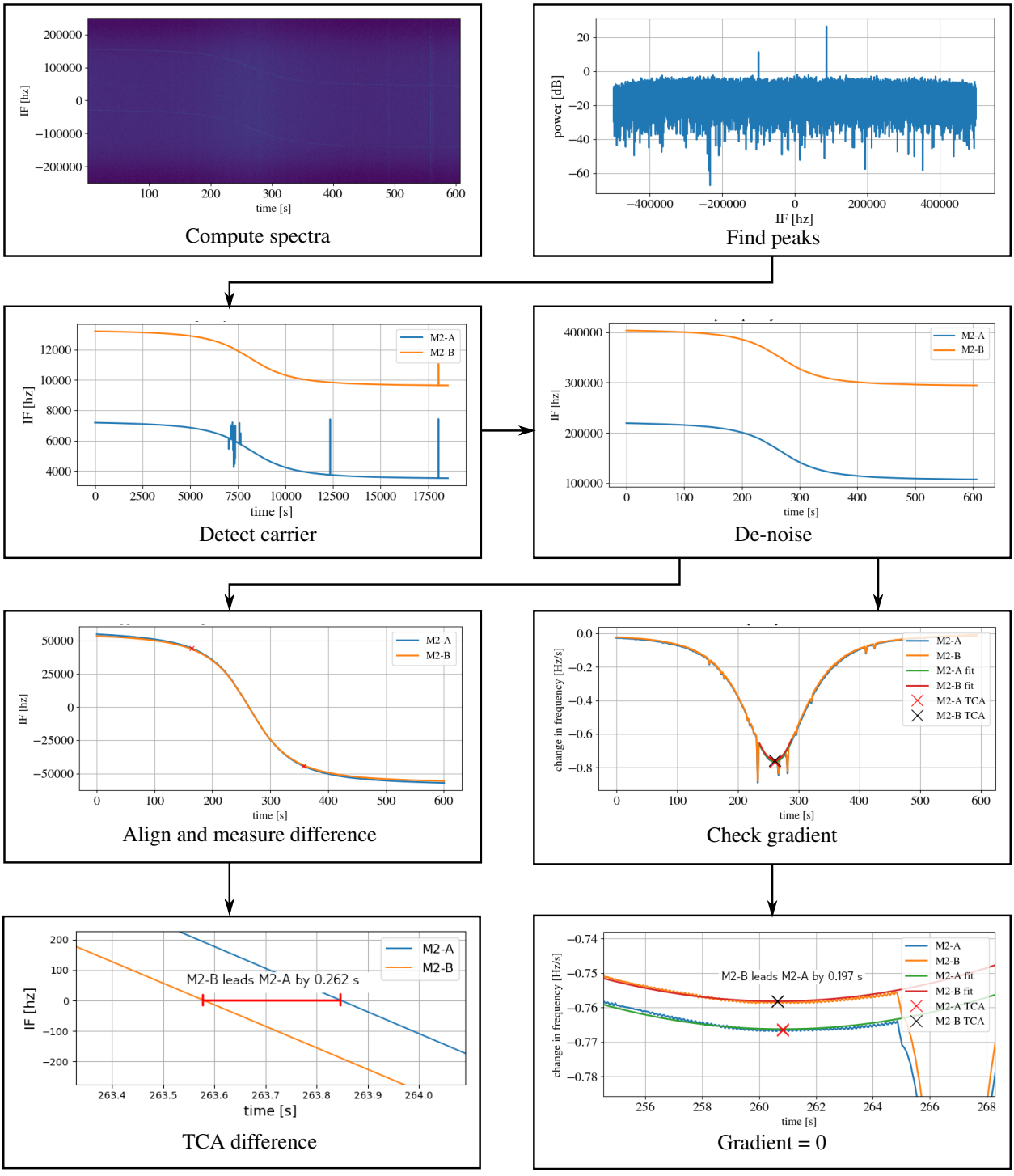

Fig. 8: The process of determining the distance between the spacecraft using passive RF data collected that feature the transmitted S band carriers.

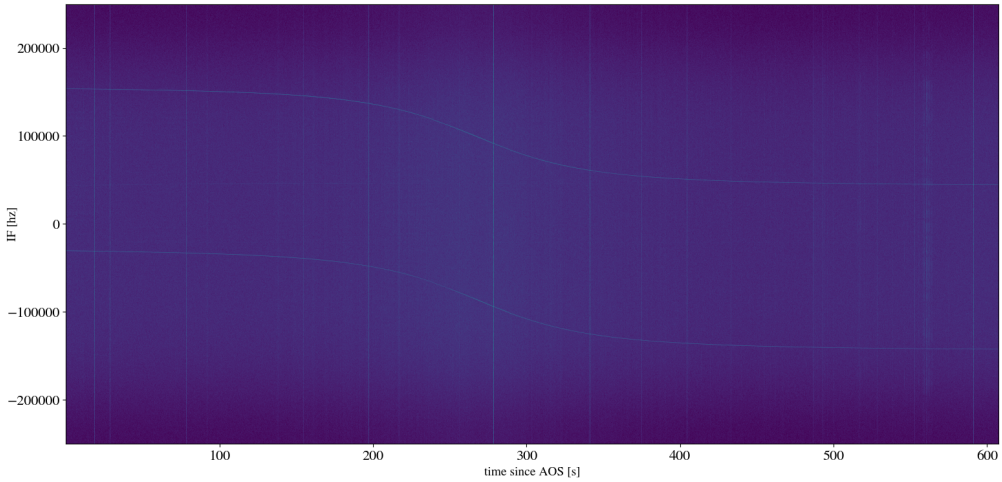

Fig. 9: A spectrogram of the RF recording of one of the S band passes recorded using the 3 m parabolic antenna at our Yass ground station. The AOS was 2022-08-03 7:42.

peaks block in Fig. 8 shows the magnitude squared of a 16 384-point fast Fourier transform (FFT). The locations of the peaks in each side of the spectrum are found. A weighted average between the neighbours is computed for a more accurate frequency estimation. The FFT frequency resolution is 30.5 Hz per bin with a time resolution of 32.8 ms. The un-smoothed frequencies throughout the pass are shown in the *detect carrier* block in Fig. 8. Disturbances are found using a gradient filter and are replaced by linear interpolations. A low-pass filter is applied to smooth the ripples from the *find peaks*. This is shown in the *de-noise* block in Fig. 8. Two methods were used to determine the difference in TCA. For the first method, the two Doppler curves were aligned and the time difference between the 0 Hz. This is shown in the *align and measure difference* and *TCA difference* blocks in Fig. 8. For the second approach, the rate of change in the Doppler is computed, and the steepest rate of change was measured. This happens at the TCA, where the Doppler rate is changing the fastest. However, due to measurement and quantisation noise in the FFT, the Doppler rate data is noisy. De-noising has been performed using a Gaussian curve fit to part of the data, discarding data that was affected by interference. This method is depicted in the *check gradient* blocks in Fig. 8.

6.2.2 Results

The Doppler estimations of the RF passes using the Doppler alignment method, illustrated graphically in the bottom left of Fig. 8 are shown in Fig. 10 shows the Doppler curves aligned with a zoomed in version at TCA for the pass with AOS at 2022/07/27 16:56. Figures 11 and 12 show the TCA section of the aligned Doppler curves from the passes at AOS 2022/08/02 14:32 and 2022/08/03 7:49. The data clearly shows that initially M2-A is leading M2-B and the distance decreases. At the 3rd of August, M2-B has passed M2-A and is now leading by 262 ms. The results using the Doppler gradient method are shown in Figs. 13 to 15. The results are summarised in Table 1. It is worth noting, that while the two TCA difference methods yield different separation estimates, both methods agree on which spacecraft is leading the formation. Future work will provide a detailed analysis of the RF data and combine this with ODs to provide more accurate estimations of the separation distance.

6.2.3 Attitude information from SNR

Monitoring the SNR of the signals during the pass revealed information on the pointing state between the spacecraft and the ground station receiver. The SNR is expected to increase between AOS and TCA and decrease between TCA and loss of signal (LOS) due to the decrease and increase in range. However, any other changes in the SNR can be caused by a variety of sources, such as:

- Ground station tracking

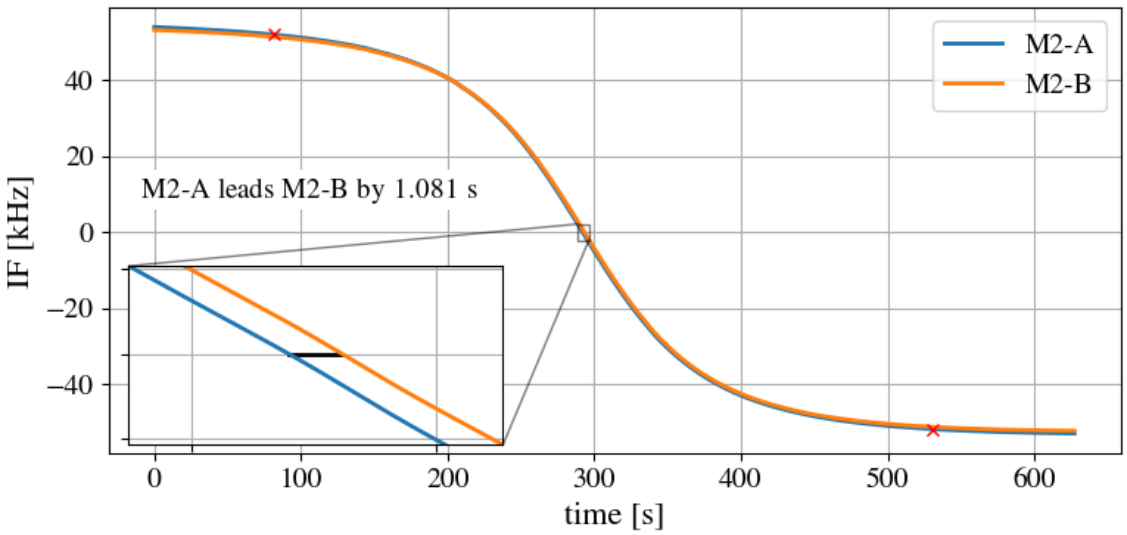

Fig. 10: Frequency difference for pass at AOS 2022/07/27 16:56.

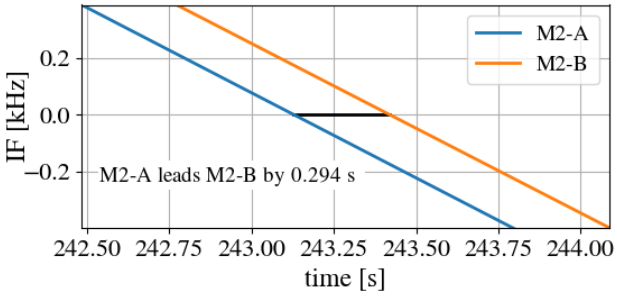

Fig. 11: Zoom of the pass at AOS 2022/08/02 14:32 with M2-A leading M2-B.

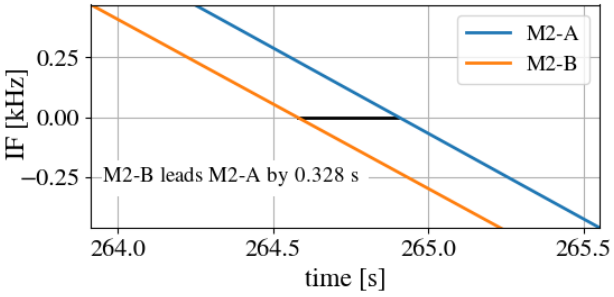

Fig. 12: Zoom of the pass at AOS 2022/08/03 7:49 with M2-B leading M2-A.

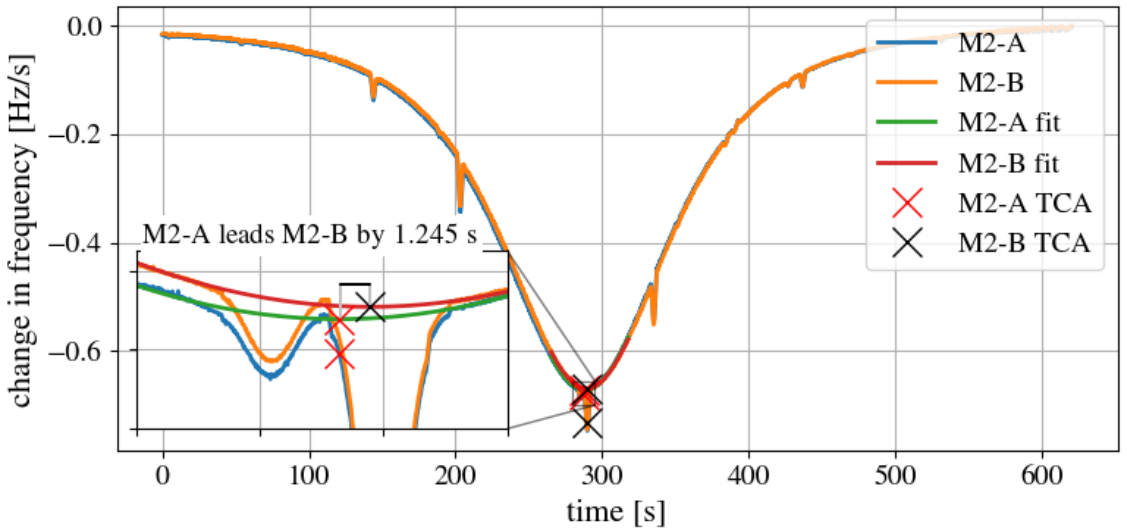

Fig. 13: Doppler rate difference for pass at AOS 2022/07/27 16:56.

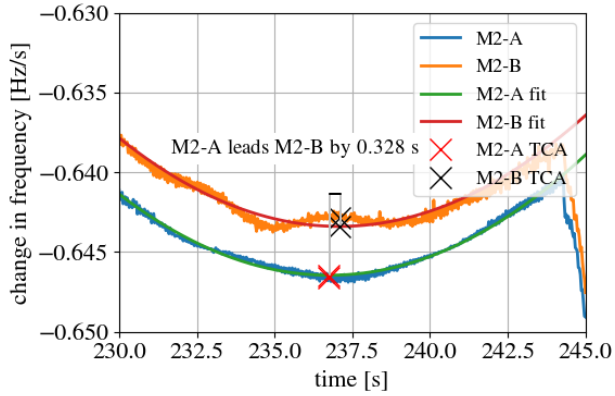

Fig. 14: Zoom of Doppler rate difference for pass at AOS 2022/08/02 14:32.

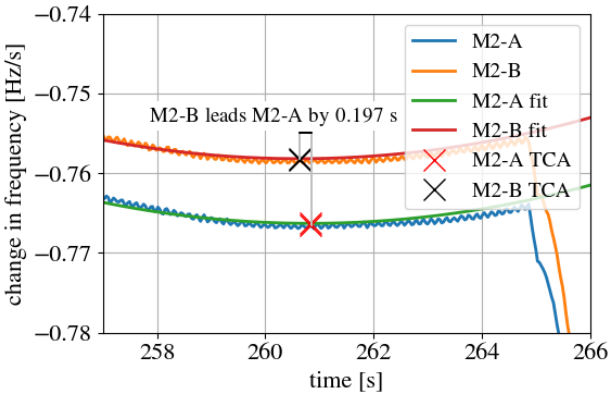

Fig. 15: Zoom of Doppler rate difference for pass at AOS 2022/08/03 7:42.

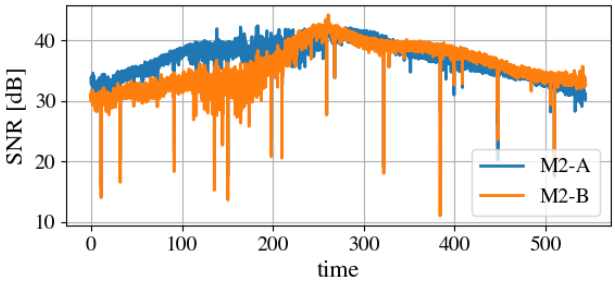

Fig. 16: SNR of the carriers with both M2-A and M2-B pointing towards the ground station.

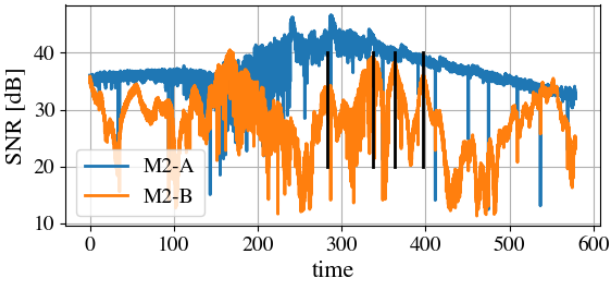

Fig. 17: SNR of the carriers with M2-A pointing towards the ground station and M2-B tumbling. Black lines mark peaks.

- Spacecraft pointing
- Varying power on the emitted RF carrier.

The SNR during a pass where both spacecraft are tracking the ground station successfully and the ground station is tracking sufficiently accurate is shown in Fig. 16. While there are minor disturbances, the SNR increases by 12 dB from AOS to TCA due to the reduction in range. The peaks in the SNR plot of M2-A in Fig. 17 are expected to be caused by tracking errors on the ground station. During these passes the TLE was used for the antenna positioner, and the TLEs during these manoeuvres was known to be inaccurate. This is expected to also be the cause for the flat line in the SNR of M2-A during the first 150 s of the pass.

The M2-B spacecraft entered an unexpected tumble shortly before the 2022/08/02 14:32 pass. Indications of this are present in the SNR plot shown in Fig. 17, where M2-A's SNR looks smooth with a few peaks, the SNR of M2-B is showing rapid but smooth changes. These changes are expected to be caused by the spacecraft tumbling. Due to the 60° radiation pattern of the on-board S-band antenna, it is non-trivial to predict the tumble rate of the spacecraft based on the data shown in Fig. 17. However, there is a pattern marked with the black lines where the interval between a peak and a dip is between 27 s to 34 s or integer multiples thereof. This could indicate a rotation around one or multiple of the spacecraft axes or a pointing error on the spacecraft where it fails to track the ground station successfully.

6.3 Optical observations of M2 with Falcon and VIPER

Optical imaging has been utilised to obtain light curve information, positioning and, when sufficiently close, the distance between the spacecraft. Figures 18 to 21 show the images captured using the Canberra Falcon telescope viewfinder. Table 2 shows the distances in pixels and the distance in km computed from the angular resolution of both the UNSW Falcon and Viper telescopes. The images in Figures 22 to 24 show the images collected using the Viper telescope.

Date and time [UTC]	Align method	Doppler rate method
2022/07/27 16:56	1.081 s (7.870 km)	1.245 s (9.064 km)
2022/08/02 14:32	0.295 s (2.148 km)	0.328 s (2.388 km)
2022/08/03 7:42	−0.328 s (−2.386 km)	−0.196 s (−1.427 km)

Table 1: Estimated distance in time and km for the RF passes. Negative values indicate M2-B leading M2-A. The orbital velocity used to compute the distance is estimated from the TLE to 7.28 km/s.

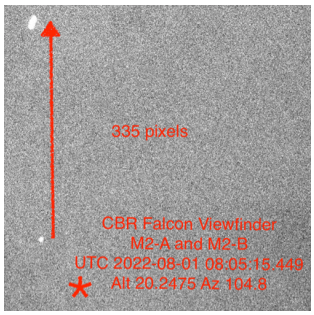

Fig. 18: Falcon viewfinder 2022/08/01 8:05.

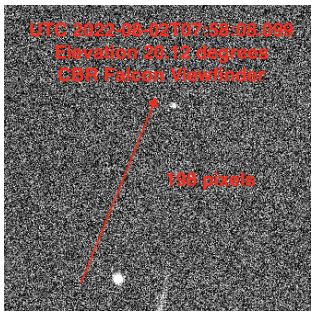

Fig. 19: Falcon viewfinder 2022/08/02 7:58.

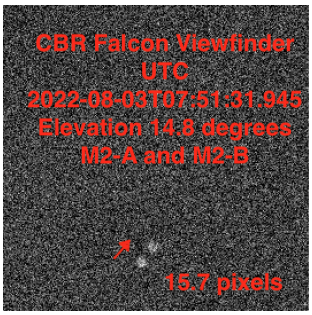

Fig. 20: Falcon viewfinder 2022/08/03 7:51.

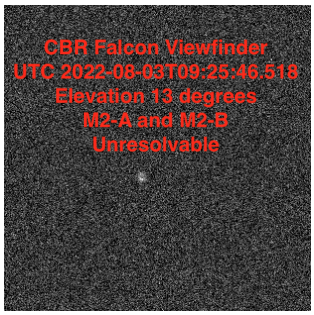

Fig. 21: Falcon viewfinder 2022/08/03 9:25.

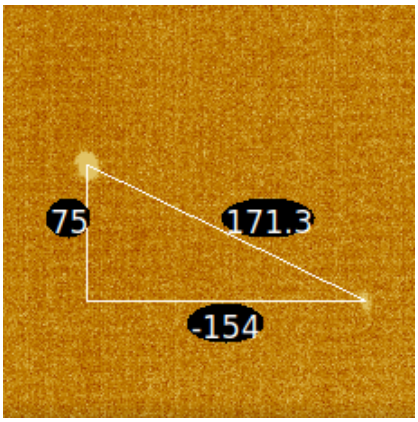

Fig. 22: Viper telescope observation at 2022/08/02 07:59 UTC with an elevation of 12.46°.

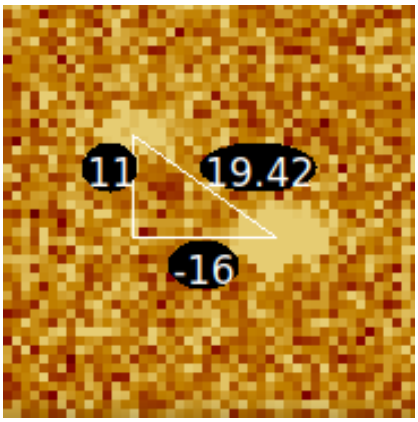

Fig. 23: Viper telescope observation at 2022/08/03 07:51 UTC with an elevation of 14.30°.

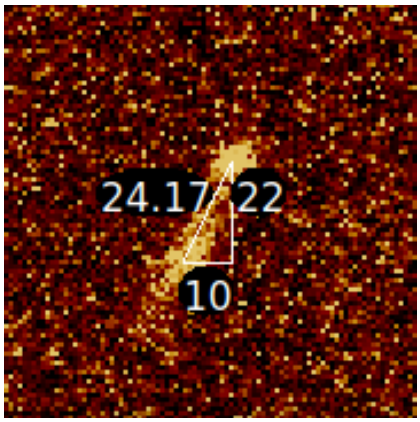

Fig. 24: Viper telescope observation at 2022/08/03 09:25 UTC with an elevation of 13.03°.

Table 2: M2 separation using Falcon optometry data. The Falcon telescope's viewfinder resolution is 9.34 µrad/pixel and Viper's resolution is 6.96 µrad/pixel

Date and time [UTC]	Distance Falcon viewfinder	Distance Viper	TLE propagation
2022/08/01 8:05	335 pixel (6.9 km)	X	5.08 km
2022/08/02 7:58	198 pixel (4.92 km)	171.3 pixel (1.93 km)	2.9 km
2022/08/03 7:51	15.7 pixel (0.8 km)	19.42 pixel (0.206 km)	0.33 km
2022/08/03 9:25	M2-A and M2-B unresolvable	24.17 pixel (0.22 km)	0.16 km

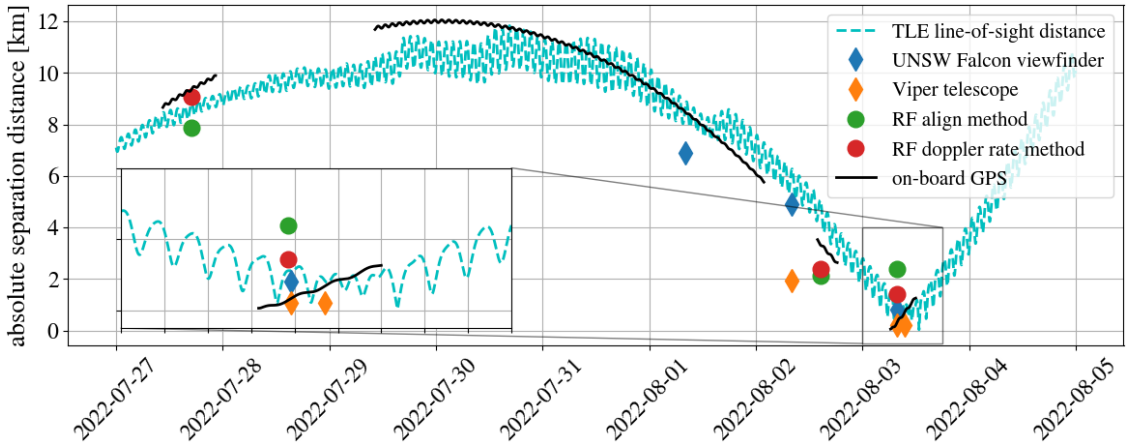

Fig. 25: The line-of-sight separation distance between the spacecraft determined using the proposed methods and computed from GPS data collected on-board the M2-A and M2-B spacecraft. The TLE line-of-sight distance is added for comparison.

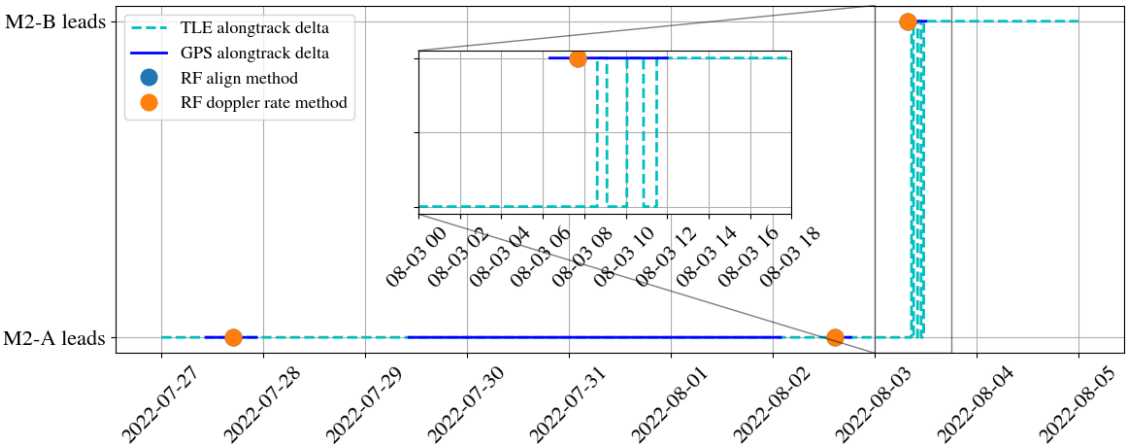

Fig. 26: The spacecraft leading the formation derived from the along track distance between M2-A and M2-B.

6.4 Analysis

The estimated line-of-sight distances between the M2-A and M2-B spacecraft are summarised in Fig. 25. The TLE line-of-sight distance between the spacecraft is computed through the 2-norm from the difference of the TLE propagations of each spacecraft. The TLE is generally shown to have an error of up to multiple kilometers, and is not designed to track manoeuvres such as change of drag. The GPS collected on-board has an error in the range of 30 m. From Fig. 25, the residual between the optical and RF observations ranges from 100s of Meters to 2 km.

The spacecraft leading the formation is shown in Fig. 26. The lead is determined from the along track distance between the spacecraft of the TLEs and on-board GPS data. The on-board GPS indicates the crossover occurred before 2022/8/3 6:20, while the first crossover according to the TLE occurred 8:38 the same day. Both passive RF observations indicate that M2-B leads the formation at 7:42 according to Fig. 26.

It is worth recalling that while both the optical and passive RF based methods are preliminary and utilised within short time during the SACT event, the difference between the results tend to lie within 3 km for the optical observation and 2 km. The TLE has an expected error of multiple kilometers.

7. FUTURE WORK

This section indicates a number of focus areas for the next stage of the CRC-P project.

7.1 Simultaneous widefield optical and RF collection on LEO constellations

Current observational methods are not synchronised between optical and RF signal collection. The Starlink constellation provides a suitable test experiment where OD can be performed using both optical and passive RF data to identify individual satellites from a field of possible sources that are visible simultaneously.

7.2 Coordinated RF observations across geographically dispersed sites

Significant computing coordination and a control framework is needed to transition from individually controlled and scheduled RF observations at a number of sites to a single point of scheduling and result analysis. A part of the CRC-P project aims to develop such a capability, supporting both RF and optical observations.

7.3 Un-cued wideband RF observations

Current RF observations are limited as SDR captures are scheduled individually with tailored centre frequency and narrow relative capture bandwidth. A wide bandwidth continuous capture with real-time object detection and filtering based on RF signatures would allow multiple objects to be detected and tracked simultaneously.

7.4 Detailed analysis of the SACT22-3 Event

The data analysis of the SACT case-study was performed live during the event. A further, in detail study awaits which will involve more advanced signal processing and analysis of the optical telescope data. OD tools will be utilised to provide more accurate information on the position and separation of the spacecraft during the manoeuvre and machine learning based light curve inversion techniques applied to better characterise the spin stability of the spacecraft during the event.

8. CONCLUSION

In this work, we presented the progress of a new STM sensor network that observes spacecraft using optical and passive RF measurements. Early results show successful collections using the optical telescopes and passive RF sensors, as well as parameter estimation, such as Doppler frequency and distance of objects as well as the optical elevation angle. An OD using range rate information extracted using a novel Doppler estimation algorithm is performed for SARAL with measurement errors around 0.5 m/s upon convergence.

A case study is provided where passive RF and optical sensors have been utilised to detect manoeuvres and the separation distance between the two UNSW Canberra Space built and operated M2-A and M2-B spacecraft. While the analysis has been performed within hours after the data has been collected, the results show a clear change in the distance between the spacecraft, and through identification of the RF carrier offset, the reversal of the order of the spacecraft could be detected successfully. Additionally, body stability of the spacecraft has been detected using SNR information extracted from passive RF data.

9. ACKNOWLEDGEMENTS

This research was funded by the Australian Government through the round 9 Cooperative Research Centre Project (CRC-9) scheme.

[1] I. Ali, N. Al-Dhahir, and J. E. Hershey. Doppler characterization for LEO satellites. *IEEE Transactions on Communications*, 46(3):309–313, Mar 1998.

[2] Francis K. Chun, Roger D. Tippets, David M. Strong, Devin J. Della-Rose, Daniel E. Polsgrove, Kimberlee C. Gresham, Joshua A. Reid, Casey P. Christy, Mark Korbitz, Joel Gray, Stanton Gartin, David Coles, Ryan K. Haaland, Russ Walker, Jared Workman, John Mansur, Victoria Mansur, Terry Hancock, Julia D. Erdley, Thomas S. Taylor, Richard A. Peters, Christopher X. Palma, William Mandeville, Steven Bygren, Christian Randall, Kevin Schafer, Tim McLaughlin, José Luis Nilo Castellón, Amelia Cristina Ramirez Rivera, Hector Andres Cuevas Larenas, Andrew Lambert, Manuel Cegarra Polo, David Blair, Mark Gargano, Jan Devlin, Richard Tonello,

Carsten Wiedemann, Christopher Kebschull, and Enrico Stoll. A new global array of optical telescopes: The falcon telescope network. *Publications of the Astronomical Society of the Pacific*, 130(991):095003, July 2018.

[3] Liu Congfeng and Yun Jinwei. A joint TDOA/FDOA localization algorithm using bi-iterative method with optimal step length. *Chinese Journal of Electronics*, 30(1):119–126, 2021.

[4] Giacomo Curzi, Dario Modenini, and Paolo Tortora. Large constellations of small satellites: A survey of near future challenges and missions. *Aerospace*, 7(133), 2020.

[5] Joseph D Gerber, Yann Picard, Melrose Brown, Dr. Jason Held, Frederic Pelletier, and Timothy Fuller. Sprint advanced concept training (SACT), a renaissance in collaborative international space operations. In *Advanced Maui Optical and Space Surveillance Technologies Conference*, September 2020.

[6] Mohd Noor Islam, Thomas Q. Wang, Samuel Wade, Travis Bessell, Tim Spitzer, and Jeremy Hallett. Doppler and angle of arrival estimation from digitally modulated satellite signals in passive RF space domain awareness. In *Advanced Maui Optical and Space Surveillance Technologies Conference*, 2021.

[7] NASA. Orbital debris, May 2021. `nasa.gov/mission_pages/station/news/orbital_debris.html`.

[8] Union of Concerned Scientists. Satellite database, May 2022. `https://www.ucsusa.org/resources/satellite-database`.

[9] Brian O'Keefe. Finding location with time of arrival and time difference of arrival techniques. *ECE Senior Capstone Project*, 2017.

[10] Edwin G. W. Peters, Timothy Bateman, Rabbia Saleem, Melrose Brown, and Andrew Lambert. A software defined radio based method for accurate frequency estimation for space domain awareness in real-time. In *Advanced Maui Optical and Space Surveillance Technologies Conference*, September 2022.